Submitted to the 29th International Conference on High-Energy Physics ICHEP98,
Vancouver, Canada, July 1998.

Charged Particle Cross Sections in Photoproduction

H1 Collaboration

Abstract

Photoproduction data collected with the H1 experiment at HERA in 1994 are used to study inclusive charged particle cross sections and the structure of the photon. The inclusive charged particle cross sections show a clear dependence on the parton densities in the photon and on higher order effects, phenomenologically interpreted as multiple interactions.

Abstract 551
Parallel sessions: 5,3
Plenary sessions: 7,5

1 Introduction

The observation that the photon has hadronic structure was first made more than 30 years ago when the cross sections of hadronic photoproduction interactions were first demonstrated to have dependences on energy and momentum transfer which were similar to hadron-hadron interactions [1]. With the advent of the quark-parton model, and subsequently QCD, more quantitative predictions for this hadronic structure became available, and their gross features were identified experimentally in e^+e^- interactions [2]. Subsequently these features have also been identified in hard photoproduction processes [3-15].

Measurements of the photon structure functions in e^+e^- interactions are directly sensitive to the quark structure of the photon. Only through QCD evolution studies can information be extracted concerning the gluon component of this structure. Recently studies of jets and high p_T charged particles in photoproduction events at the ep collider HERA have shown sensitivity to the partonic content of the photon. Here the photon structure is probed by partons of the proton, rather than by a virtual photon as in $e\gamma$ collisions. Hence these data are sensitive to both the quark and gluon content of the photon. Leading order diagrams are shown in Fig. 1, for so called direct (Fig. 1a; the photon couples directly to the partons in the proton) and resolved (Fig. 1b; the partons of the hadronic component of the photon scatter on the partons of the proton) processes in photoproduction. In Leading Order (LO) only the latter process contains information on the partonic structure of the photon.

In [5] inclusive charged particle production has been studied. It was established that the data, in particular the tail at large transverse momentum, p_T, can be described by Next-to-Leading order QCD calculations. The charged particle distributions as function of the pseudorapidity, $\eta = -\ln\tan(\theta/2)$, with θ the polar angle of the particle in the HERA laboratory frame [1], were found to be sensitive to the partonic structure of the photon. In this paper we present data based on an event sample sample which is 50 times larger than the one used in [5].

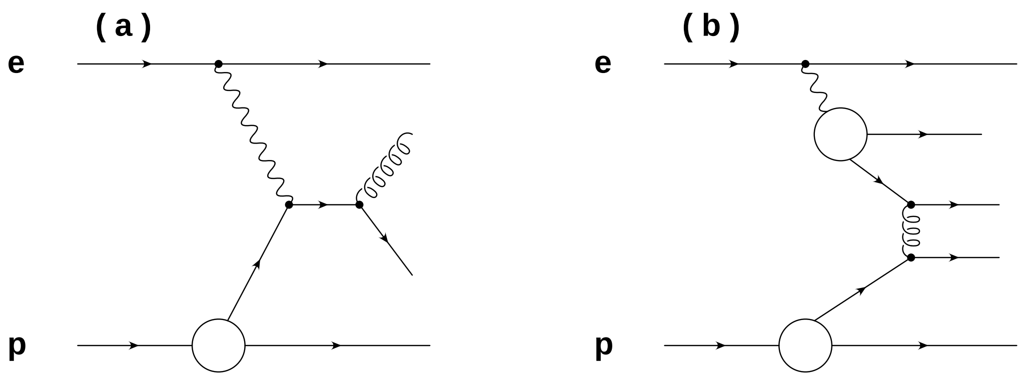

Figure 1: Examples of diagrams for direct (a) and resolved photon (b) processes in ep scattering.

[1]Polar angles are measured with respect to the proton beam.

2 Experimental Setup

The data are collected with the multi-purpose detector H1 [16] at the HERA collider. Positrons of 27.5 GeV collide on protons of 820 GeV. The total data sample corresponds to 1.35 ± 0.02 pb^{-1}.

A detailed description of the H1-detector has been given elsewhere [16]. Here only the components crucial for this particular analysis will be described.

The H1 luminosity system consists of an electron detector and a photon detector, located 33 m and 103 m from the interaction point in the electron beam direction (backward, i.e. downstream with respect to the electron beam), respectively. The luminosity is determined from the rate of Bethe-Heitler $ep \to ep\gamma$ events by detecting the photon. Both detectors are TlCl/TlBr crystal Čerenkov calorimeters with an energy resolution of $10\%/\sqrt{E}$. The electron detector is used to tag photoproduction events by detecting electrons scattered at small angles.

Measurements of charged tracks are provided by two cylindrical drift chambers [17], mounted concentrically around the beamline inside a homogeneous magnetic field of 1.15 Tesla. Up to 65 space points are measured for a track yielding particle charge and momentum from the track curvature in the polar angular range of 20° and 160°. The resolution for the momentum measurement in the $x - y$ plane transverse to the beam direction (p beam in $+z$ direction) is $\sigma(p_T)/p_T \sim 0.6\% p_T$ (GeV/c^{-1}) in the p_T range considered hereafter. The resolution for the polar angle θ is 2 mrad.

The central tracking system is complemented by a forward tracking system. All trackers are surrounded by a fine grained liquid argon sampling calorimeter , consisting of an electromagnetic section with lead absorbers and a hadronic section with steel absorbers.

3 Data Analysis

3.1 Event Selection and Background Reduction

Photoproduction events are selected which have the scattered electron detected in the electron tagger, and consequently have a four momentum transfer $Q^2 < 10^{-2}$ GeV^2,where $Q^2 = 4E_eE'_e\cos^2(\theta/2)$. Here E_e and E'_e are the incoming and scattered electron energy and θ the polar angle of the scattered electron. Tagged events are required to have an electron candidate in the fiducial volume of the electron-tagger with energy $E_{e'} > 4$ GeV and to have less than $E_\gamma < 2$ GeV deposited in the photon detector. The latter condition suppresses p-background, which appears in a random coincidence with the high rate Bethe-Heitler events, and also reduces initial state QED corrections. In addition a track-based trigger is required, which is formed using only 10 selected layers out of 56 radial signal wire layers of the CJC. It allows to find the presence of at least one negative charge track with $p_T > 700$ MeV/c and which has a distance of closest approach to the nominal beam line of less than 2 cm from the nominal beam axis; this requirement suppresses beam-wall events as well as synchrotron radiation background.

For this analysis the events are required to have $0.3 < y = E_\gamma/E_e < 0.7$ where E_γ and E_e are the photon and electron beam energies respectively. As a consequence, the γp centre-of-mass energy range is 164.5 GeV $< \sqrt{s_{\gamma p}} <$ 251.3 GeV, with an average of $\sqrt{s_{\gamma p}} \sim 200$ GeV. An interaction vertex, reconstructed using tracks in the central tracker (CT), has to be within 30 cm of its nominal position. These events were triggered with an energy deposit in the electron tagger in coincidence with a negatively charged track reconstructed by the drift chamber trigger.

A total of about 960000 events satisfy all described criteria. The remaining background is determined by analysing data from electron pilot bunches (i.e. electron bunches which have no colliding proton bunch partner) and from a monitoring subtrigger of minimum bias events. It is found to be less than 2.7 % at this stage of selection, before tighter cuts on track quality and transverse momentum are applied.

3.2 Track Selection

For this analysis, tracks from the central tracker are selected which have a transverse momentum with respect of the beam axis of at least 2.0 GeV/c, a pseudorapidity measured in the HERA reference system of $|\eta| < 1$ and a minimum track length of 30 cm in the $x - y$ plane. The latter cut is essential to ensure a good measurement of p_T of the track, from 2 up to 12 GeV/c, which is the range considered here. To minimize the systematic errors, sectors of the CT in ϕ which have shown a lower efficiency have been excluded from the analysis. A total of 16591 tracks has been selected for the analysis, resulting from 15543 events.

3.3 Corrections

In order to obtain the produced number of tracks, $N_{produced}$, the observed number of tracks is corrected with the following factors:

- A_{etag} : The geometrical acceptance of the electron tagger is corrected for per event, as a function of y and amounts to 55 % in average for $0.3 < y < 0.7$. The tagger efficiency within the chosen acceptance is 100 %.
- ϵ_{trig} : The CJC trigger efficiency has been estimated from a sample of minimum bias e-tagged events. For the high p_T range considered here, it is found to be 96.3 ± 1.2 %, independent of p_T, η and ϕ.
- ϵ_{event} : Three components in the event efficiency have to be considered : (i) The restriction of the primary event vertex to $-25 < z_V < +35$ cm, which corresponds to a 3 σ cut around the average position of the interaction point, is taken into account in the estimation of the integrated luminosity used for this analysis. (ii) The residual background from beam-gas, beam-wall, and pile-up events, after demanding a well-measured, high p_T track such as defined above, is found to be negligible. (iii) The background from cosmic events is removed by rejecting events with two opposite charge tracks meeting the requirements above (except for ϕ region cut), and which are aligned in θ and ϕ to better than 5^o. All events rejected by this cut were visually checked and confirmed to be cosmic events, and all were found to have at least one track with $p_T > 6$ GeV/c. Reversely, all events with at least one track with $p_T > 6$ GeV/c were visually scanned and no further cosmic event was found. A check for potential contamination from DIS overlap events was also performed : no such events were found. The total event efficiency amounts to $\epsilon_{event} = 100$ %.
- ϵ_{track} : The overall track efficiency contains four multiplicative components : (i) The efficiency for finding and reconstructing single tracks, ϵ_{rec}, is from Monte Carlo and found to be 99.2 ± 0.8 %. The agreement between data and Monte Carlo has been verified by visual scanning of tracks in both samples. (ii) The efficiency of the cut on transverse track length, $\epsilon_{\Delta R}$, is estimated from data to be 97.9 ± 0.4 %. This was checked to be independent of both η and ϕ. (iii) The ϕ-restriction, ϵ_ϕ, of the geometrical acceptance of the central drift chamber is accounted for assuming a uniform distribution in ϕ, and amounts to 53.1 %. (iv) Finally the bin-to-bin migration in p_T, ϵ_{mig}, due to the fast decreasing p_T

spectrum and to the finite resolution in p_T ($dp_T/p_T = 0.6$ % p_T), was estimated from a Monte Carlo simulation and found to be $103.8 \pm 1.3\%$, independent of p_T. The total ϵ_{track} is then 53.5 $\pm 1.6\%$, where the systematic errors have been added in quadrature.

Detailed checks and comparisons with Monte-Carlo led the introduction of an extra systematic error, to account for a remaining p_T measurement uncertainty, which showed up in two ways : in the ratio of positively and negatively charged tracks and in the efficiency of a harder transverse track length cut ($\Delta_R > 50$ cm). The resulting uncertainty was estimated to be parameterized as $2\% \cdot p_T$ at the center of each bin for p_T distributions, and as $2\% \cdot p_T^{low}$ for η distributions with $p_T > p_T^{low}$. All systematic uncertainties are added in quadrature.

The overall uncertainty of 5the electron tagger acceptance has to be added to the systematic errors, and is not included in the error bars shown in the figures below.

4 Monte Carlo Simulation Programs

The PYTHIA 5.7 event generator [18] was used to simulate photon-proton interactions. As well as the leading-order cross section, PYTHIA includes initial- and final-state parton radiation effects which are calculated in the leading logarithmic approximation. The strong coupling constant α_s is calculated in first order QCD using $\Lambda_{\rm QCD} = 200\,\rm MeV$ for 4 quark flavours. Multiple parton interactions were generated in addition to the primary parton–parton scattering. They are calculated as leading-order QCD processes between partons from the photon and proton remnants. The transverse momentum of all parton–parton interactions was required to be above $p_T = 1.2\,\rm GeV$. This cut-off value (p_T^{min}) has been found to give an optimal description of the transverse energy flow outside the jets [19]. LAC1 and GRV-LO parameterizations were used for the parton distributions of the photon and GRV-LO for the proton [20, 21]. Hadronization was modelled with the LUND string fragmentation scheme (JETSET 7.4 [22]).

Since the kinematics of the hard scattering process will be related to the p_T values of the particles with high transverse momentum, it is imperative to study the fragmentation dependence of this measurement. A model with a different hadronization scheme, HERWIG [23] was used for this purpose. In this model the hadronization is based on cluster fragmentation. Other parameters, such as the parton densities for the photon and proton are taken the same as for PYTHIA. Both the LUND model and HERWIG were found to give a good description of the general features of fragmentation as measured in e^+e^- collisions at LEP.

The model calculations the parton distributions of the proton from the GRV distributions are used, while for the photon several different sets have been used: GRV, SAS1D and LAC1. All these parametrizations are QCD fits to photon structure function data measured in $e\gamma$ collisions, but have different assumptions for the gluon content, which is only weakly constrained by these measurements. In particular LAC1 assumes a large gluon content of the photon at small-x values.

5 Inclusive Charged Particle Cross Sections

The invariant cross section for single particle production is given by

$$\frac{\mathrm{d}^2\sigma}{\mathrm{d}p_T^2\,\mathrm{d}\eta} = \int \frac{\mathrm{d}^3\sigma}{\mathrm{d}p_T^2\,\mathrm{d}\eta\mathrm{d}\phi} \cdot \mathrm{d}\phi = \pi \cdot E \cdot \frac{\mathrm{d}^3\sigma}{\mathrm{d}p^3} \qquad (1)$$

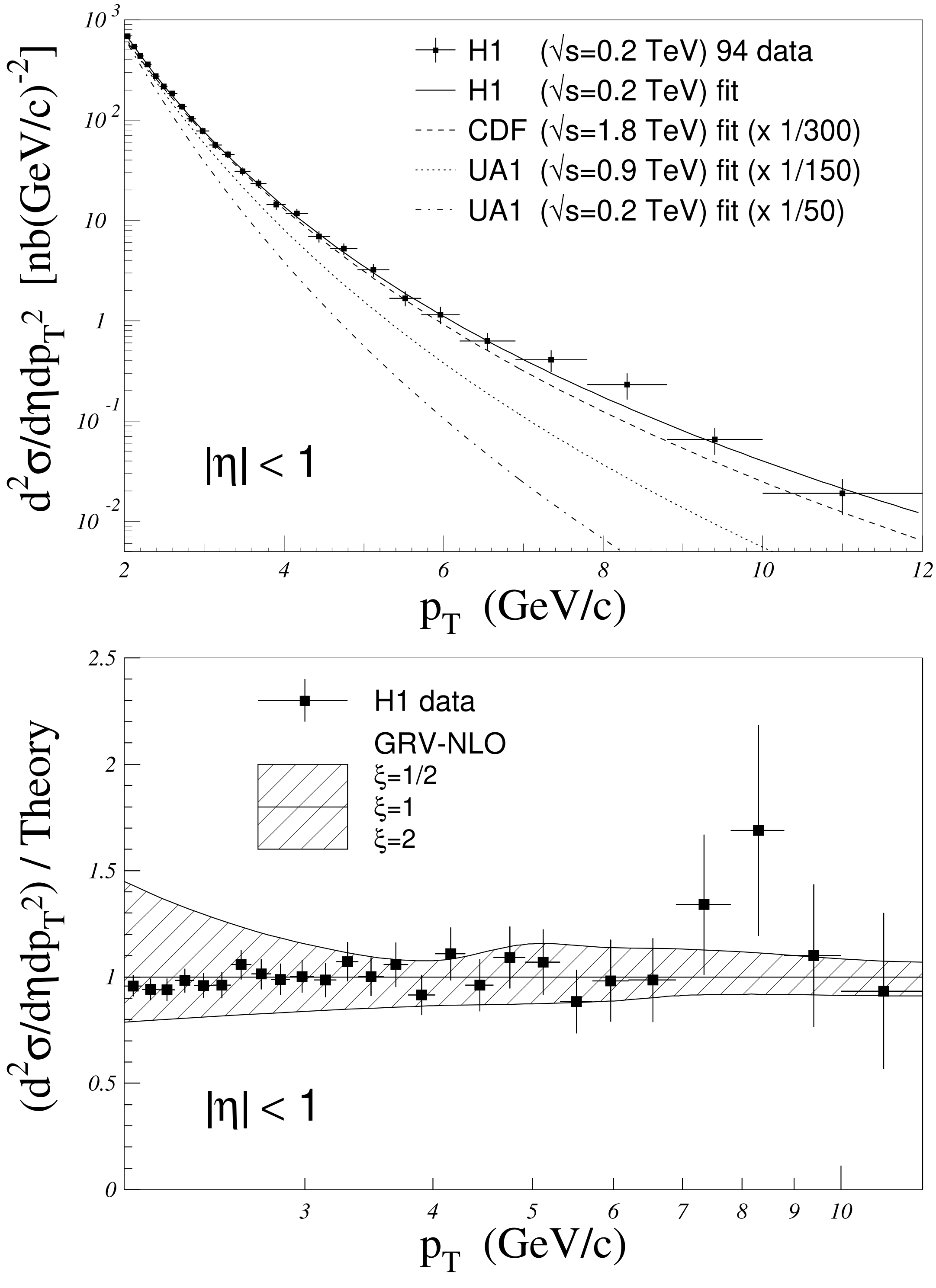

Figure 2: **(a)** The inclusive γp cross section for charged particles in photoproduction (full dots) measured in the kinematical region $\mid \eta \mid < 1.5$ at an average $E_{CMS}(\gamma p) \approx 200$ GeV. The error bars indicate the quadratic sum of statistical and systematic errors. An overall uncertainty of 5% from the luminosity measurement and the electron tagger acceptance is not included in the figure. The curves indicate power-law fits, as described in the text, for our data and for the $p\overline{p}$ data from UA1 and CDF **(b)** The ratio of data over NLO QCD calculations with scale ξp_T.

assuming azimuthal symmetry of the cross section and thus allowing the integration over ϕ. The cross section for inclusive charged particle production in γp collisions is calculated from

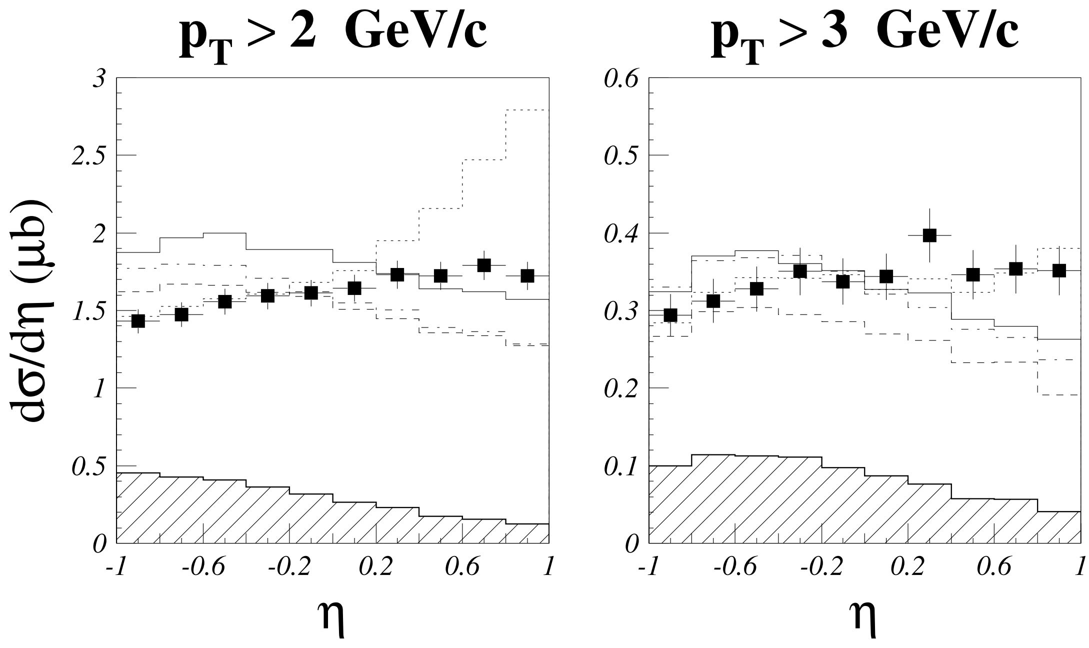

Figure 3: The differential γp cross section $d\sigma/d\eta$ for inclusive production of the high p_T charged particles (dots) in comparison with LO QCD calculation by PYTHIA (histograms). Different lines represent different photon structure function parametrisations: GRV with (full) and without (dash-dotted) multiple interactions, SAS1D (dashed) and LAC1 (dotted). The contributions from the direct photon processes are shown as shaded histogram.

the number of tracks produced, $N_{produced}$, in a bin of p_T and η by applying all efficiency and acceptance corrections to the observed track spectrum. It is given by :

$$\frac{\mathrm{d}^2\sigma}{\mathrm{d}p_T^2\ \mathrm{d}\eta} = \frac{f N_{produced}(p_T, \eta)}{\mathcal{L} \cdot 2p_T \Delta p_T \cdot \Delta\eta} \tag{2}$$

where $\mathcal{L}$ denotes the integrated luminosity and f photon flux according to $\mathrm{d}\sigma = \sigma(\gamma p) \cdot Flux(y) \cdot \mathrm{d}y$. For the chosen y-range the integral over y of the photon flux yields a factor 0.0136, assuming the Weizsäcker-Williams approximation [24]. $\Delta\eta$ and $\Delta p_T^2 = 2 \cdot p_T \cdot \Delta p_T$ are the bin widths.

The resulting differential cross section for positively and negatively charged particles is shown in fig. 2a. The error bars denote the quadratically combined systematic and statistical errors. The data exhibit a strong improvement in precision compared to the previous H1 measurement [5] and cross sections are now given up to 12 GeV/c in p_T. The QCD inspired power-law [25] expression

$$E \cdot \frac{\mathrm{d}^3\sigma}{\mathrm{d}p^3} = A \cdot (1 + \frac{p_T}{(p_T)_0})^{-n}. \tag{3}$$

is fitted to the data. The fitted curve is presented in Fig. 2a. The fit gives $A = 17.1 \pm 2.1$ mbarn and n=7.03 ± 0.07 (statistical errors), with a $\chi^2/NDF = 8.8/24$. The parameter $(p_T)_0$ was fixed to the value 0.63, as found in [5], but other values in the range 0.5–0.75 were found

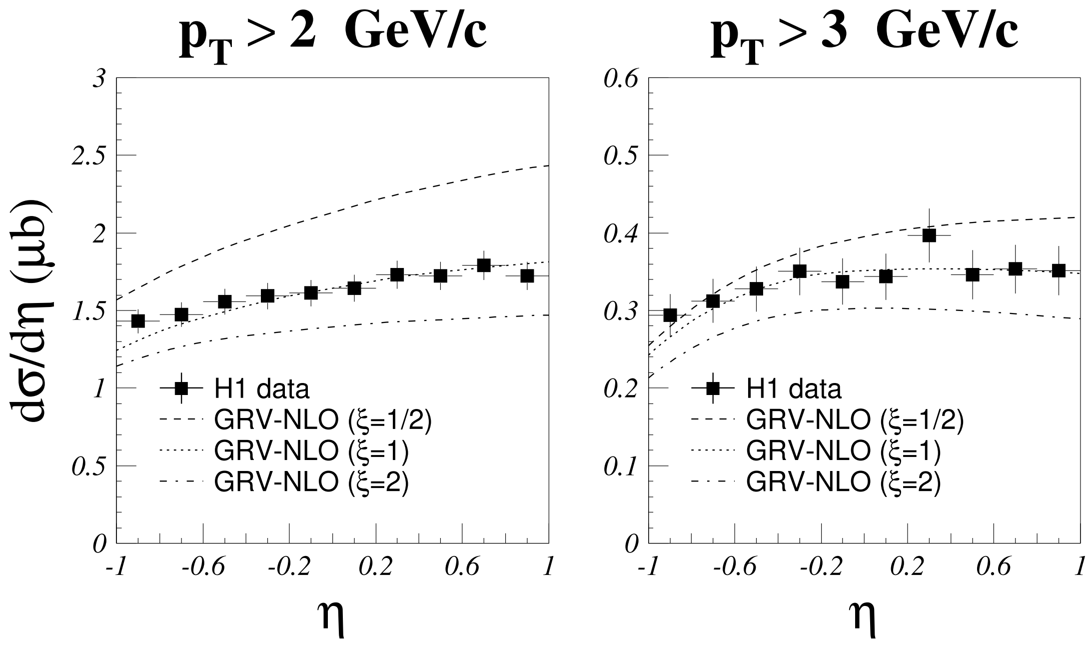

Figure 4: The differential γp cross section $d\sigma/d\eta$ for inclusive production of the high p_T charged particles (dots) in comparison with NLO QCD calculations, with different values of the scale, taken as $\mu = \xi p_T^2$

to give equally good fits. The effect of the choice of $(p_T)_0$ leads the an uncertainty on the power n of about 0.2.

In the same figure 2a are shown the results of similar fits through the data of UA1-collaboration [26] at the $\bar{p}p$ collider at $\sqrt{s} = 200$ and 900 GeV in the rapidity region $\eta <| 2.5 |$, and data of CDF[27] at $\sqrt{s} = 1800$ in the rapidity region $\eta <| 1 |$, scaled by the factors indicated in the figure, which essentially normalizes all data to the γp cross section at $p_T = 2$ GeV. In the γp CMS system the H1 data overlap with this rapidity interval in the photon hemisphere. The high p_T tail is observed to increase with increasing energy in $\bar{p}p$. The hardness of the γp spectrum is comparable to that of the the $\bar{p}p$ data from CDF. This can be understood as being due to extra contributions in γp, namely the direct and pointlike resolved component[5].

In Fig.2b the ratio of data to the Next-to-Leading order calculation [28] prediction using GRV structure functions for photon and proton. For the scale p_T^2 is chosen, and the effect of this choice is shown by predictions for a scale of ξp_T^2, with $\xi = 0.5$ and 2. The calculations describe the data well.

The dependence of the cross section on the pseudorapidity η, $\mathrm{d}\sigma/\mathrm{d}\eta$, is shown in fig. 3 for all particles with $p_T > 2.0$ and 3.0 GeV/c. Note, that the η measured in the HERA frame is on average shifted by 2 units with respect to the η^* distribution in the γp CMS system. The spread of this shift due to the photon energy range is less than 0.3 units in pseudorapidity. Therefore the η and η^* distributions look very similar. The data are consistent with being flat in most of the region, with a possible decrease towards $\eta = -1$, i.e. in the photon direction. The data are compared with predictions of LO QCD calculations made with PYHTIA, for different structure functions of the photon and assumptions on the soft interactions in the underlying events.

Predictions are shown for GRV with (full) and without (dash-dotted) multiple interactions, SAS1D (dashed) and LAC1 (dotted). All these structure functions are still compatible with the present available data. The contributions from the direct photon processes are shown as shaded histogram and decrease when moving more towards the proton direction. For the data with $p_T > 2$ GeV/c, there is a strong sensitivity to the parton distributions in the photon, but also to the amount of underlying interactions as shown by the GRV curves. None of the scenarios presented shows a satisfactory agreement with the data. For data with $p_T > 3$ GeV/c the effect of multiple interactions becomes very small, as shown for the GRV predictions. The sensitivity to the photon structure is reduced but still significant. The data agree best with LAC1, and disagree with SAS1D. It was checked that these results do not depend on the choice of the parton distributions of the proton, when selected among those consistent with the most recent proton structure function data.

In Fig.4 the cross sections as function of η are compared with NLO calculations, including direct and resolved contributions. The NLO calculations[28] reproduce the data, however one can see a considerable effect of the QCD scale on both the shape and normalization of the distribution, as shown by the curves for different ξ values. The effect is substantially smaller for data with $p_T > 3$ GeV/c. The scale has been also identified as the reason for the considerable difference between the LO and NLO GRV cross section prediction. PYTHIA uses as a scale the p_T of the hard partonic interaction, while the program of [28] uses the p_T of the final state particle, which can be considerably different from the original parton.

6 Summary

High p_T charged tracks measured in photoproduction events with the H1 detector at HERA have been measured. The p_T spectra exhibit a high p_T tail, larger than in $p\bar{p}$ collisions at similar and higher center of mass system energy. The η spectra show sensitivity to the parton densities in the photon. When charged particles down to $p_T = 2GeV$ are included, there is also a significant effect from the activity in the underlying event.

Acknowledgements

We are grateful to the HERA machine group whose outstanding efforts have made and continue to make this experiment possible. We thank the engineers and technicians for their work in constructing and now maintaining the H1 detector, our funding agencies for financial support, the DESY technical staff for continual assistance, and the DESY directorate for the hospitality which they extend to the non-DESY members of the collaboration.

References

[1] J.J. Sakurai, Ann. Phys. 11, (1960) 1;
M. Gell-Mann and F. Zachariasen, Phys. Rev. 124, (1961) 953.

[2] PLUTO Collab., Ch. Berger et al., Nucl. Phys. B281 (1987) 365.
JADE Collab., W. Bartel et al., Z. Phys. C24 (1984) 231.
TASSO Collab., M. Althoff et al., Z. Phys. C31 (1986) 527.
TPC/2γ Collab., H. Aihara et al., Z. Phys. C34 (1987) 1.
AMY Collab., S.K. Sahu et al., Phys. Lett. B346 (1995) 208.
TOPAZ Collab., K. Muramatsu et al. Phys. Lett. B332 (1994) 477.
DELPHI Collab., P. Abreu et al., Z. Phys. C69 (1996) 223.
OPAL Collab., K. Ackerstaff et al., Z. Phys. C74 (1997) 33.

[3] H1 Collab., I. Abt et al., Phys. Lett. B297 (1992) 205.

[4] H1 Collab., I. Abt et al., Phys. Lett. B314 (1993) 515.

[5] H1 Collab., I. Abt et al., Phys. Lett. B328 (1994) 176.

[6] H1 Collab., T. Ahmed et al., Nucl. Phys. B445 (1995) 195.

[7] H1 Collab., S. Aid et al., Z. Phys. C70 (1996) 17.

[8] H1 Collab., C. Adloff et al., Eur. Phys. J. C1 (1998) 97.

[9] ZEUS Collab., M. Derrick et al., Phys. Lett. B297 (1992) 404.

[10] ZEUS Collab., M. Derrick et al., Phys. Lett. B322 (1994) 287.

[11] ZEUS Collab., M. Derrick et al., Phys. Lett. B342 (1995) 417.

[12] ZEUS Collab., M. Derrick et al., Phys. Lett. B348 (1995) 665.

[13] ZEUS Collab., M. Derrick et al., Z. Phys. C67 (1995) 227.

[14] ZEUS Collab., M. Derrick et al., Phys. Lett. B384 (1996) 401.

[15] ZEUS Collab., J. Breitweg et al., Eur. Phys. J. C1 (1998) 109.

[16] H1 Collab., I. Abt et al., Nucl. Instr. and Methods A386 (1997) 310.
H1 Collab., I. Abt et al., Nucl. Instr. and Methods A386 (1997) 348.

[17] J. Bürger et al., Nucl. Instr. and Methods A279 (1989) 217.

[18] T. Sjöstrand, CERN-TH-6488 (1992), Comput. Phys. Commun. 82 (1994) 74.

[19] H1 Collab., S. Aid et al., Z. Phys. C70 (1996) 17.

[20] M. Glück, E. Reya and A. Vogt, Phys. Rev. D46 (1992) 1973.

[21] M. Glück, E. Reya and A. Vogt, Z. Phys. C53 (1992) 127.

[22] T. Sjöstrand, M. Bengtsson, Comput. Phys. Commun. 43 (1987) 367.

[23] G. Marchesini and B.R. Webber et al., Comp. Phys. Comm. 67 1992 465.

[24] C.F.Weizsäcker, Z. Phys. 88 (1934) 612; E.J.Williams, Phys. Rev. 45 (1934) 729.

[25] R. Hagedorn, Riv. Nuovo Cim. 6 (1983) 1.

[26] UA1 Collab., Albajar, C. et al., Nuc. Phys. B 335 (1990) 261.

[27] F. Abe et al., Phys. Rev. Lett. 77 (1996) 438. CDF Collab., to be filled in.

[28] F.M.Borzumati, B.A.Kniehl and G.Kramer, Z. Phys. C 59 (1993) 341. B.A.Kniehl and G.Kramer, DESY 94-009 (1994).
B.A.Kniehl private communication